Journal of Power Sources, *34* (1991) 339–352

Silver arsenate amorphous electrolyte batteries: conduction characteristics and electrochemical performance

P. Sathya Sainath Prasad*

Corrosion Research Center, Department of Chemical Engineering & Materials Science, University of Minnesota, Minneapolis, MN 55455 (U.S.A.)

B. Rambabu

Surface Physics & Materials Science Laboratory, Department of Physics, Southern University, Baton Rouge, LA 70813 (U.S.A.)

(Received August 21, 1990; in revised form November 8, 1990)

Abstract

Transport properties of silver ion conducting ternary amorphous solid electrolytes, XAgI–[$(1-X)(y$Ag$_2$O–zAs$_2$O$_3$)] and XAgI–[$(1-X)(y$Ag$_2$O–zAs$_2$O$_5$)] for $30 \leqslant X \leqslant 70$ mol% AgI and $0.20 \leqslant (z/y) \leqslant 3.0$ were characterized in a two step process to determine the highest ion conducting composition. Interesting results were obtained by the variation of Glass Former to Glass Modifier ratio (z/y) and AgI content (X). Some of the results were previously reported with z/y as a variable parameter for a constant concentration of X. The values of z/y were maintained at the best conducting compositions as derived from the previous work, and the present study reports the conduction characteristics with X as a variable parameter. The best conducting amorphous electrolytes in these two systems were used in the fabrication of solid-state batteries, and their electrochemical performance has been evaluated. A comparison of the solid-state cells with amorphous and polycrystalline electrolytes was undertaken with regard to the current discharge profiles and the cell capacities.

1. Introduction

Anion substituted AgI–Ag_3AsO_4, AgI–Ag_3VO_4, AgI–Ag_3PO_4, AgI–Ag_2MoO_4, AgI–Ag_2CrO_4 and AgI–Ag_2WO_4 have been the most studied materials in the family of silver ion conducting solid electrolytes [1–6]. This group of solid electrolytes based on silver iodide and silver oxysalts was characterized by high ionic conductivity at ambient temperature and, hence, is termed as superionic conductors (SIC) or fast ion conductors (FIC). Polycrystalline and amorphous forms of the above binary systems have also been studied in the extended pseudo binary or ternary form as AgI–Ag_2O–B_2O_3, AgI–Ag_2O–V_2O_5, AgI–Ag_2O—P_2O_5, AgI–Ag_2O–MoO_3 and AgI–Ag_2O–CrO_3 with the advantage of achieving a large number of electrolytes by the continuous variation of

*Author to whom correspondence should be addressed. Present address: Building No. 480, Materials Science Division, Brookhaven National Laboratory, Upton, Long Island, NY 11973, U.S.A.

0378-7753/91/$3.50

solid state chemical composition [7–10]. The role of each component in a ternary amorphous solid electrolyte is identified as a superionic conductor (AgI), glass modifier (Ag_2O) and a glass former (B_2O_3, V_2O_5, P_2O_5, MoO_3 and CrO_3). The criteria for choosing an amorphous electrolyte as solid-state battery material were established to be the stability of the electrolyte, high ionic conductivity, low electronic conductivity, and low polarization effects when compared with their polycrystalline counterparts. The most important parameter that determines the temperature region in which the solid-state ionic device can be operated is determined to be the glass transition temperature (T_g) of the amorphous electrolyte.

Hence, to identify new amorphous electrolytes with high T_g, apart from B_2O_3-based systems [7], other glass forming oxides such as As_2O_3, Bi_2O_3, Sb_2O_3, and Nb_2O_5, which seem to have remarkable stability at high temperature, were also investigated. Thus work in this direction has been progressive with the transport and surface analysis of silver arsenate glasses that belong to $AgI–Ag_2O–As_2O_3$ and $AgI–Ag_2O–As_2O_5$ [11]. On studying the transport properties of polycrystalline and amorphous solid electrolytes in the systems XAgI–$[(1-X)(y Ag_2O–z As_2O_3)]$ and XAgI–$[(1-X)(y Ag_2O–z As_2O_5)]$, we reported that amorphous electrolyte compositions with 66.67 mol% of AgI, and a glass former (GF) to glass modifier (GM) ratio of 1.0 in the former system, have a high ionic conductivity of 2.00×10^{-2} S cm^{-1} with a very low electronic conductivity of 2.10×10^{-8} S cm^{-1} at ambient temperature [11]. In continuation of our previous studies, the present investigation involves an attempt to understand the role of AgI on the transport behavior of the electrolytes by maintaining z/y ratio at the best conducting compositions, i.e., at 1.0 and 0.50, respectively, in the above mentioned systems. The highest conducting compositions are used as electrolyte materials in the fabrication of solid-state electrochemical cells. The cells are characterized by studying the variation of open circuit voltage (OCV) with temperature, current discharge profiles, load discharge characteristics, and anode/electrolyte, cathode/electrolyte polarization effects at the interfaces.

2. Experimental

2.1. Electrolyte preparation

Solid electrolytes, XAgI–$(1-X)(1.0\ Ag_2O–1.0\ As_2O_3)$ and XAgI–$(1-X)(2.0\ Ag_2O–1.0\ As_2O_5)$ in the ternary systems $AgI–Ag_2O–As_2O_3$ and $AgI–Ag_2O–As_2O_5$, for $30\leqslant X\leqslant 80$ mol% were prepared from Analar-grade chemicals AgI, Ag_2O (AR grade, Sigma Inc., U.S.A.) and anhydrous As_2O_3, As_2O_5 (AR grade, Aldrich Inc., U.S.A.) by mixing the appropriate quantities to the required composition. Electrolytes were prepared by a novel method of preparation, as discussed in our earlier publication [11]. The ingredients were pestled to a fine mixture and melted in a quartz crucible at 1200 K for 4 h. The homogeneous melt was quenched by passing a fine stream of liquid nitrogen in the zone-controlled quenching apparatus. Another set of

electrolytes corresponding to the same compositions have been prepared by allowing the melt to attain ambient temperature by a slow cooling process, by which polycrystallinity is anticipated.

Electrolytes prepared by both the methods were characterized by recording X-ray diffractograms on 1.0 g of each electrolyte sample with Cu Kα radiation using a PW 1140 X-ray diffractometer. Rapidly quenched electrolytes were found to possess featureless, peak-free X-ray diffractograms, demonstrating the amorphous nature, where the nucleation due to crystallization was hindered by the rapid quenching. Electrolytes were found to be amorphous only for the compositions $40 \leqslant X \leqslant 66.67$ mol% of AgI in the AgI–Ag_2O–As_2O_3 system and $35 \leqslant X \leqslant 66.67$ mol% of AgI in the AgI–Ag_2O–As_2O_5 system. Beyond these limits, electrolytes demonstrated polycrystalline nature where the diffraction peaks due to the wurtzite form of AgI have been reflected in both the systems. The second set of electrolytes, which were allowed to cool down to ambient temperature, showed distinctive and intense peaks in the X-ray diffractograms. These peaks could not be resolved any further but for the existence of polycrystallinity.

2.2. Conductivity measurements

Ionic conductivity measurements were undertaken on pulverized electrolytes using an electrode mixture of silver powder (400 mesh) and electrolyte powder in 1:4 ratio by weight. Electrolytes were pressed into pellets of 1.3 cm dia. under 5000 kg cm^{-2} using a Perkin-Elmer hand press. Conductivity measurements were performed at 1.0 kHz frequency using a GR 1689 Precision LCR digibridge in the 295–390 K temperature range.

Electronic conductivity measurements were performed on pulverized electrolytes in the Wagner's d.c. polarization cell of the configuration (−Ag)/(Electrolyte)/(C+), where carbon acts as an ion blocking electrode [13]. When d.c. potentials less than the decomposition potential of the electrolyte are applied, a current flow would be set up in the circuit. Initially silver ions migrate towards the silver electrode and a depletion of silver ions occurs at the elecrolyte/graphite electrode interface. Under steady state conditions, the concentration gradient due to ion migration balances the external applied potential gradient. The conduction of silver ions is suppressed and the current flow would be due to either electrons or holes, or both. Under equilibrium or steady-state conditions, the current response of the cell was measured by applying d.c. potentials in the range 10–200 mV. At each applied potential, a steady-state current was reached after 4–5 h which was measured with a Keithley 485 autoranging picoammeter.

2.3. Cell fabrication

Typical solid-state cells used in the present investigation consist of three compartments, namely, anode, electrolyte, and a cathode. The anode material was prepared from metallic silver powder and finely pulverized electrolyte powder in a 1:1 ratio by weight. The mixture was placed into an evacuable die of 1.3 cm dia. and on applying a pressure of 2500 kg cm^{-2}, a thin

pellet was obtained. Electrolyte powder was spread uniformly as a thin layer on the surface of the anode pellet. The anode pellet and electrolyte layer were pelletized together under a pressure of 5000 kg cm^{-2}. In a separate mortar, granular iodine, electrolyte powder, and graphite powder were finely pulverized in a 5:1:5 ratio by weight for the preparation of the cathode material. The cathode was pressed into a separate pellet of 1.3 cm dia. Amalgamated silver anodes were prepared by mixing silver powder, electrolyte powder, and mercury in a 1:1:1.008 ratio by weight. A complete cell was fabricated by pressing the anode–electrolyte pellet onto the thin cathode pellet of the same diameter to achieve the configuration (anode)/(electrolyte)/(cathode). These solid-state electrochemical cells were then loaded into metal cans and crimped to form a crimp-sealed unit using a Jonco battery fabrication machine. Polypropylene carbonate sheet material was used as an insulation gasket between the bottom anode case and the top cathode case of the button cell.

3. Conduction characteristics

3.1. Ionic conductivity measurements

Figures 1 and 2 indicate the variation of the logarithm of ionic conductivity with the inverse of absolute temperature for the electrolytes XAgI–$(1-X)$[Ag_2O–As_2O_3] and XAgI–$(1-X)$[2.0 Ag_2O–1.0 As_2O_5], $30 \leqslant X \leqslant 70$ mol%. The variation of ionic conductivity with temperature follows Arrhenius behavior, satisfying the equation

$$\sigma = \sigma_o/T \exp(-E_a/kT) \quad (1)$$

where σ_o is the pre-exponential factor, T is the absolute temperature, k is the Boltzmann constant, and E_a is the activation energy for silver ion migration.

The ionic conductivity increases linearly with silver iodide content (X) in the amorphous matrix until $X = 66.67$, and decreases thereon. All the paths for $X > 50$ mol% converge at higher temperatures. An inquisitive insight into the solid electrolytes was due to the need to stabilize the high temperature, highly conductive α-phase of AgI at ambient temperature in the presence of As_2O_3 and As_2O_5 glass forming structures appropriately modified by Ag_2O. The influence of glass former to glass modifier ratio (GF/GM) on silver ion conduction mechanism has already been discussed in our earlier papers [11, 12]. Thus, silver ion motion is visualized in a sub-phase of iodide ions which surround the oxyanionic framework formed by Ag_2O–As_2O_3 and Ag_2O–As_2O_5. At 50 mol% of AgI, which also corresponds to 50 mol% of (Ag_2O–As_2O_3 or Ag_2O–As_2O_5), a balance of charge with I^- ions occurs, since the network hosts one Ag^+ ion per one silver atom partially covalently connected with As_2O_3 or As_2O_5 polyhedral structures. The observation of highest ionic conductivity,and the glass forming limit for 66.67 mol% of AgI in both the systems, suggest the glassy networks capability to host more than one silver ion per covalently bonded silver to the oxyanionic network. Thus, any further

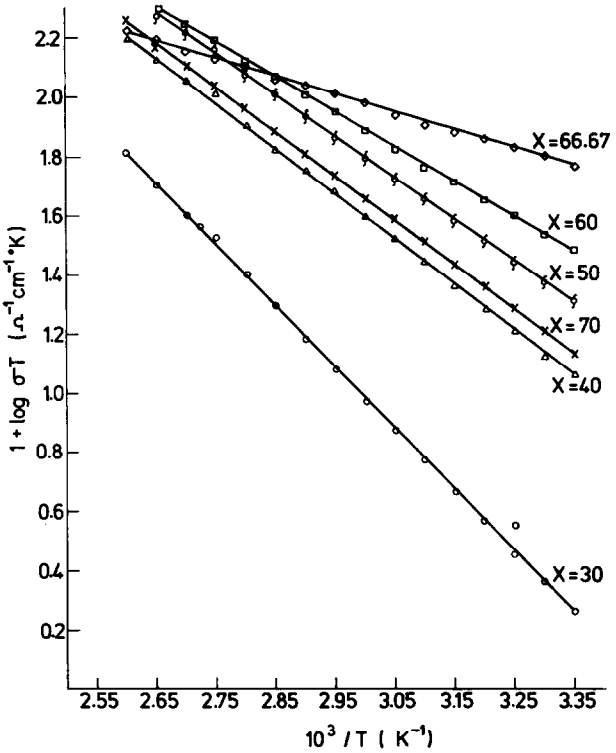

Fig. 1. Variation of conductivity with temperature in Arrhenius coordinates for XAgI–$(1-X)(Ag_2O–As_2O_3)$ electrolytes where $X=30$ (○), 40 (△), 50 (§), 60 (□), 66.67 (◇), and 70 (×).

addition of AgI other than 66.67 mol% would likely coalesce with the I^- sub-phase already present in the glassy structure. In all compositions of the electrolyte with AgI > 66.67 mol%, excessive 'undissolved' β-AgI reflections were observed in the X-ray diffractograms. Even though the upper limit of AgI that could be retained in the structure remains the same in both systems, the lower limits were 40 and 35 mol% in the As_2O_3 and As_2O_5 systems, respectively. Beyond these limits, electrolytes possess a polycrystalline nature corresponding to β-Ag I structure reflections. It is possible for the hexavalent and pentavalent arsenic networks to be completely surrounded by I^- ions only up to 40 and 35 mol%, respectively, of AgI, thus retaining an amorphous nature. For an identical concentration of AgI in both AgI–Ag_2O–As_2O_3 and AgI–Ag_2O–As_2O_5 electrolytes, the ultimate silver ionic conduction depends on the appropriate modification of the glass-forming oxide networks to facilitate silver ion migration [11]. However, on continuous variation of X in both the systems, a high ionic conductivity of the order of 2.00×10^{-2} and 1.86×10^{-2} S cm^{-1} was observed for the electrolyte compositions (mol%) 66.67 AgI–16.67Ag_2O–16.67As_2O_3 and 66.67AgI–22.22Ag_2O–11.11-As_2O_5 at 298 K. The activation energy of silver ion migration for the two

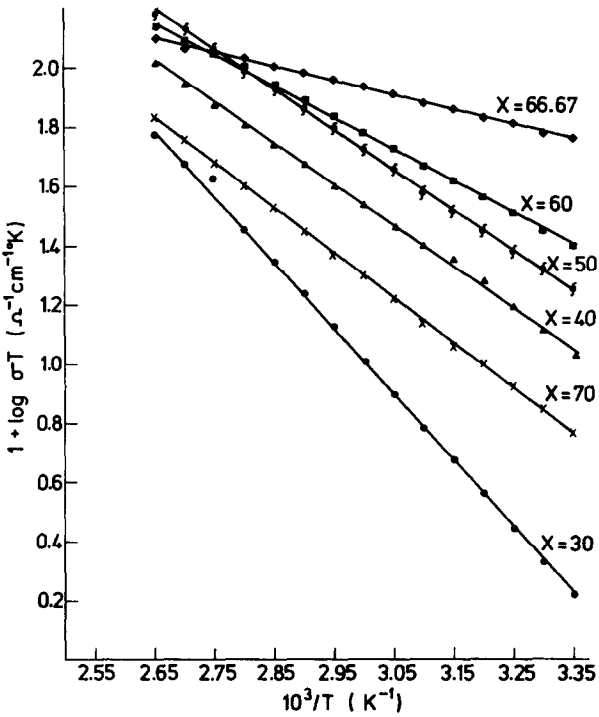

Fig. 2. Variation of conductivity with temperature in Arrhenius coordinates for XAgI–$(1-X)(Ag_2O–As_2O_5)$ electrolytes where $X=30$ (●), 40 (▲), 50 (§), 60 (■), 66.67 (♦), 70 (×).

electrolytes was determined to be 0.10 and 0.12 eV, respectively. The polycrystalline electrolytes corresponding to the best conducting amorphous electrolytes exhibit an ionic conductivity of 1.43×10^{-3} and 4.10×10^{-4} S cm^{-1}, respectively, with an activation energy of 0.18 and 0.22 eV. Polycrystalline electrolyte ionic conductivities were one and two orders of magnitude lower than their corresponding amorphous electrolytes.

The glass transition temperature (T_g) was identified, from the variation of ionic conductivity with temperature, as the point where electrical resistance of the electrolyte increases with increasing temperature. This definition of T_g is not conventional and is quite accepted in the field of Solid State Ionics. Moreover, these values are in good agreement with the results arrived at from differential thermal analysis. In Figs. 1 and 2 the variation was indicated only up to a temperature of 395 K. The increase in resistance of the electrolyte above T_g is due to the irreversible decomposition of the material into poorly conducting phases, one of which might be the wurzite form of AgI. X-ray diffraction analysis of these electrolyte pellets slowly cooled to room temperature confirmed the presence of β-AgI as one of the decomposition products. The glass transition temperatures of the best conducting electrolytes were 371 and 383 K, the latter corresponding to the As_2O_5 system. The low

ionic conducting compositions with $X = 40$ mol% in both the systems possess a high glass transition temperature of 408 and 427 K in the As_2O_3 and As_2O_5 systems, respectively. The glass transition temperature decreases with increasing AgI content in both As_2O_3 and As_2O_5 amorphous networks. This observation leads to the conclusion that, as silver iodide is inserted into As_2O_3 and As_2O_5 amorphous networks, the stronger bonds would be replaced by weaker bonds, and a structural rearrangement takes place to attain a thermodynamically stable phase. The observation of large and prominent variations of T_g values in As_2O_5-based electrolytes when compared with As_2O_3-based electrolytes is an indication of the presence of strong cross-linked polyhedra in As_2O_5-based electrolytes, since T_g depends on the number of bonds to be broken and established for a thermodynamic equilibrium.

The activation energy for Ag^+ ion migration decreases linearly as the AgI content increases in the As_2O_3 and As_2O_5 amorphous networks, as is evident from the linear plots of Figs. 1 and 2. Electrolytes with $X < 40$ and $X > 66.67$ mol% AgI are a mixture of polycrystalline and amorphous phases with higher activation energies, and those with $40 \leqslant X \leqslant 66.67$ mol% are only amorphous with lower activation energies. This is indicative of randomness in the amorphous matrix, which facilitates Ag^+ ion motion more easily when compared with polycrystalline electrolytes [11]. Thus, in both the $AgI–Ag_2O–As_2O_3$ and $AgI–Ag_2O–As_2O_5$ systems, the highest conducting compositions were noted as being for the same AgI content (66.67 mol%) and different glass formers to modifier ratios, as explained in our earlier study [12].

3.2. Electronic conductivity measurements

Figures 3 and 4 indicate the current–voltage characteristic curves of Wagner's polarization cells with As_2O_3- and As_2O_5-based electrolytes. Under steady state conditions, the current passing through the cell is given by

$$I = I_e + I_h = (RTA/LF)\ [\sigma_e(1 - \exp(-EF/RT)) + \sigma_h(\exp(EF/RT) - 1)] \quad (2)$$

where I_e and I_h are the currents due to electrons and holes, respectively, E is the applied potential, F the Faraday constant, R the Universal gas constant and L and A are the thickness and the area of the cell, respectively. According to this equation, if the conduction is only due to electrons, the current response I increases with E and saturates at higher applied potential due to the involvement of the term $(1 - \exp(-EF/RT))$. If the conduction is only due to holes, I increases exponentially with E, which results from the term $(\exp(EF/RT) - 1)$. The experimental current response of the cells shown in Figs. 3 and 4 indicates a saturation at higher applied potentials. From this saturation nature and from eqn. (2), the current carriers in these amorphous electrolytes were identified as electrons and not electron holes. Now Wagner's expression (2) for the current flowing through the cell is given by

$$I = I_e = (RTA/LF)\ \sigma_e(1 - \exp(1 - EF/RT)) \quad (3)$$

At higher potentials, where $EF \gg RT$ eqn. (3) reduces to

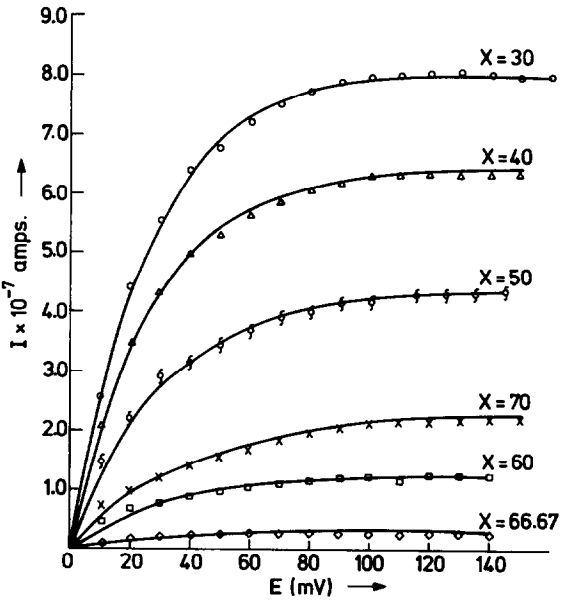

Fig. 3. Voltage–current characteristic curves for different AgI contents: $X=30$ (○), 40 (△), 50 (§), 60 (□), 66.67 (◇), 70 (×) in the amorphous electrolytes XAgI–$(1-X)(Ag_2O–As_2O_3)$.

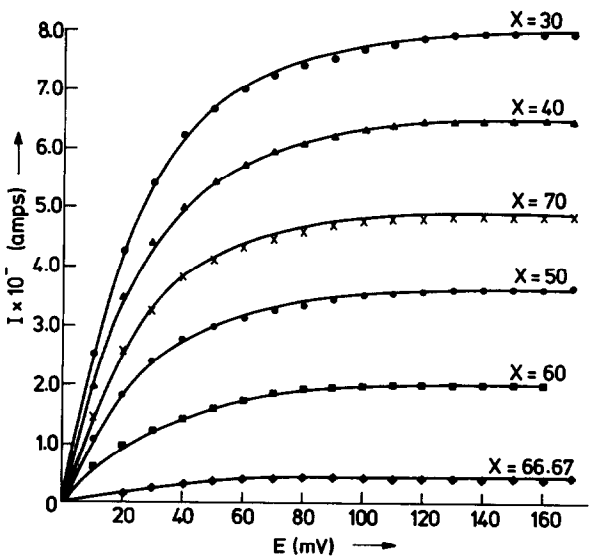

Fig. 4. Voltage–current characteristic curves for different AgI contents. $X=30$ (●), 40 (▲), 50 (×), 60 (■), 66.67 (◆), 70 (×) in the amorphous electrolytes XAgI–$(1-X)(Ag_2O–As_2O_5)$.

$$I_e \sim (RTA/LF)\ \sigma_e \qquad (4)$$

Hence the electronic conductivity was calculated by considering the saturated currents of Figs. 3 and 4. The values were counter-checked by calculating the electronic conductivity from eqn. (3) and considering the slope of I versus $1-\exp(-EF/RT)$ plots as shown in Figs. 5 and 6. The electronic conductivity of the electrolytes was of the order of 10^{-7}–10^{-8} S cm^{-1} at 298 K. The highest ionic conducting compositions possess a low electronic conductivity of 2.1×10^{-8} and 2.16×10^{-7} S cm^{-1}, respectively, in the As_2O_3 and As_2O_5 systems. The corresponding polycrystalline electrolytes possess electronic conductivities of 3.10×10^{-7} and 6.70×10^{-6} S cm^{-1}, which are one order of magnitude higher than the corresponding amorphous materials. Since the low electronic conductivity promotes the shelf life of the solid-state battery when these electrolytes are used as electrolyte materials, the highest ionic conducting compositions with low electronic conductivity is used in the fabrication of the batteries.

From the ionic and electronic conductivity values, the transport numbers of silver ions and electrons in the amorphous electrolytes were calculated to be 0.9999 and 0.0001, respectively, as described earlier [11, 12]. Even though the transport number of silver ions does not differ in any of the electrolytes, the observation of the highest ion conductivity in only two compositions, (mol%) $66.67AgI$–$16.67Ag_2O$–$16.67As_2O_3$ and 66.67AgI–

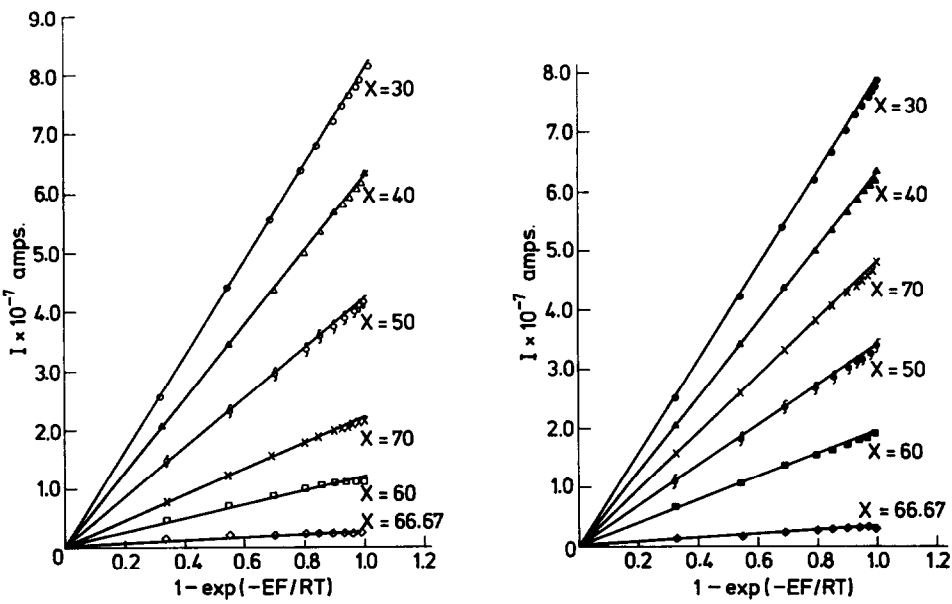

Fig. 5. A plot of current–voltage fit to Wagner's eqn. (3), for XAgI–$(1-X)(Ag_2O$–$As_2O_3)$ electrolytes, where $X=30$ (○), 40 (△), 50 (§), 60 (□), 66.67 (◇), 70 (×).

Fig. 6. A plot of current–voltage fit to Wagner's eqn. (3), for XAgI–$(1-X)(Ag_2O$–$As_2O_5)$ electrolytes, where $X=30$ (●), 40 (▲), 50 (§), 60 (■), 66.67 (◆), 70 (×).

$22.22Ag_2O–11.11As_2O_5$, suggests an increased mobility of Ag^+ ions in these compositions alone. As these two compositions fulfill the criteria for a good solid electrolyte, solid-state cells were constructed and characterized along with a comparison of the corresponding polycrystalline analogues.

4. Electrochemical performance

4.1. Open circuit voltage

The open circuit voltage of cells I, II, III, IV, V, and VI, whose electrolyte compositions are indicated below, were observed to be 678, 680, 678, 678, 663, and 666 mV, respectively. The observed values agree well with the theoretical value of 687 mV calculated from the Gibb's free energy of the cell reaction $Ag + 1/2\ I_2 \rightarrow AgI$ at 25 °C. As the change in Gibbs free energy depends on the oxidation–reduction potentials of anode and cathode materials, the observation of low open circuit voltage in the amalgamated silver anode/iodine couple indicates a lower silver activity due to amalgamation with mercury. The transport numbers of Ag^+ ions and electrons were calculated from the observed and theoretical values of the open circuit voltage for the Ag/I_2 couple. These are in good argeement with the calculated values from conductivity measurements, indicating that 99.99% of the charge is transported by ions in the electrolyte.

Cell I: (Ag)/(66.67AgI–16.67Ag_2O–16.67As_2O_3 polycrystalline electrolyte)/(I_2 + C)

Cell II: (Ag)/(66.67AgI–16.67Ag_2O–16.67As_2O_3 amorphous electrolyte)/(I_2 + C)

Cell III: (Ag)/(66.67AgI–22.22Ag_2O–11.11As_2O_5 polycrystalline electrolyte)/(I_2 + C)

Cell IV: (Ag)/(66.67AgI–22.22Ag_2O–11.11As_2O_5 amorphous electrolyte)/(I_2 + C)

Cell V: (Ag + Hg)/(66.67AgI–16.67Ag_2O–16.67As_2O_3 amorphous electrolyte)/(I_2 + C)

Cell VI: (Ag + Hg)/(66.67AgI–22.22Ag_2O–11.11As_2O_5 amorphous electrolyte)/(I_2 + C)

4.2. Discharge characteristics

Figure 7 indicates the discharge profiles of the six cells: I, II, III, IV, V and VI at a constant discharge current density of 0.15 mA cm^{-2}. The variations in discharge curves are divided into three regions where the first part corresponds to a rapid decrease in the cell potential within the first few minutes, the second region to a continuous decrease for several hours, and the third region to a steep decrease. Considering each part individually, in the first region a rapid decrease in cell potential might be due to the electrode–electrolyte polarization effects, especially at the silver anode. These polarization effects seem to be less prominent in amalgamated silver anode and amorphous electrolyte cells when compared with cells having unamal-

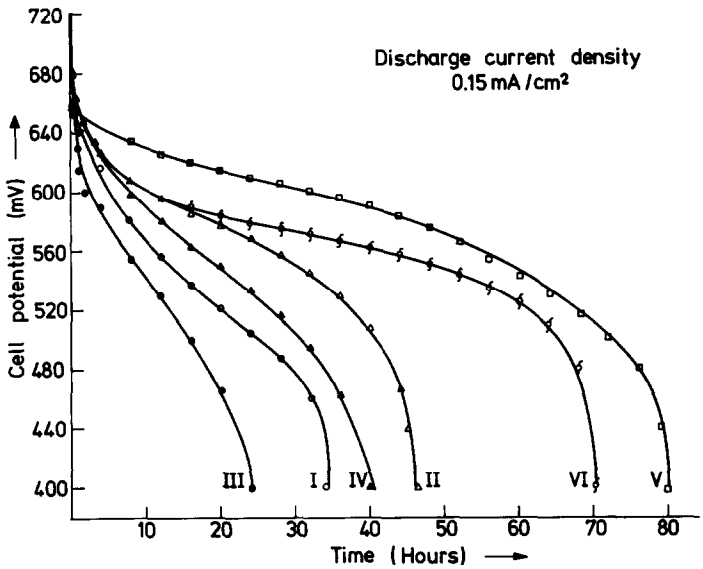

Fig. 7. Constant discharge current density plot with time for cell I–cell IV at a cut-off potential of 400 mV. Cell I curve is represented by (○) and cells II, III, and IV are represented by curves with symbols (△), (●) and (□), respectively.

gamated silver anodes and polycrystalline electrolytes. The better discharge profiles for amorphous electrolyte cells could be due to the low internal resistance of the solid electrolyte itself. In the case of polycrystalline electrolytes whose ionic conductivity is an order of magnitude less than the corresponding amorphous electrolytes, the internal resistance of the cell is high and, hence, there will be a contribution from the resistance polarization to the noticeable polarization effects at the electrolyte/electrode interface. The observation of less polarization in amalgamated silver anode cells might be due to the reaction of interstitial silver ion with mercury in which no reaction polarization could be observed whereas, in other cells, the reaction between interstitial silver ions and silver ion vacancies is the rate determining step responsible for polarization.

The variation of the internal resistance of cells II, IV, V and VI, containing an amorphous electrolyte was less compared with cells I and III, containing a polycrystalline electrolyte, after the completion of the discharge process. The increase in internal resistance of the cells after the discharge process was due to the formation of a low conducting AgI layer at the electrolyte/I_2 interface.

In order to achieve a continuous discharge with less deterioration of the cell capacity, which arises due to the large increase in the ohmic resistance after the partial discharge process, the formation of thicker AgI layers should be alleviated. From Fig. 7, the capacities of cells I, II, III, IV, V and VI are compared qualitatively and quantitatively by considering a lower cut-off voltage at 0.5 V. The calculated cell capacities are 4.06, 6.24, 2.58, 4.77,

10.58, and 9.97 mA h cm^{-2} for cells I–VI, respectively. The success of achieving higher capacity and better discharge efficiency for cells V and VI could be attributed to the implementation of amalgamated silver anodes, where the anode–electrolyte interfacial polarization is reduced, leading to a longer discharge time and also to the better transport properties of the amorphous electrolytes.

Figure 8 shows the variation of cell potential due to a 30 s pulse discharge in cells II, IV, V, and VI. Cells of types V and VI can be discharged to a current density of 500 μA cm^{-2} without polarization. Of the four cells, cell V has a high capacity and the polarization limited current is about 0.7 mA cm^{-2}. Thus, six cells of the configuration indicated in cell V were subjected to galvanostatic discharge at various current densities, as indicated in Fig. 9. The improvement in the anode–electrolyte interface in amalgamated anodes has a pronounced effect on the discharge characteristics of cells V and VI, of which cell V has the better cell capacity.

Figure 9 shows the variation of cell potential with time for cell V at various current densities ranging from 1.0 μA cm^{-2} to 0.70 mA cm^{-2}. For discharge current densities below 100 μA, the cell exhibits flat discharge profiles and, hence, has a utility in low-current-drain applications. At higher discharge current densities above 0.25 mA cm^{-2}, the cell potential decreases rapidly in the first few minutes and the discharge profiles are less flat when compared with low-drain profiles. On a comparative note, the variation of the cell potential in the first 4 h is about 120 mV at 0.68 mA cm^{-2} whereas it is only 15 mV at 1.0 μA cm^{-2}. Hence, cell V exhibits good electrochemical behavior with relatively high capacity at low discharge current densities.

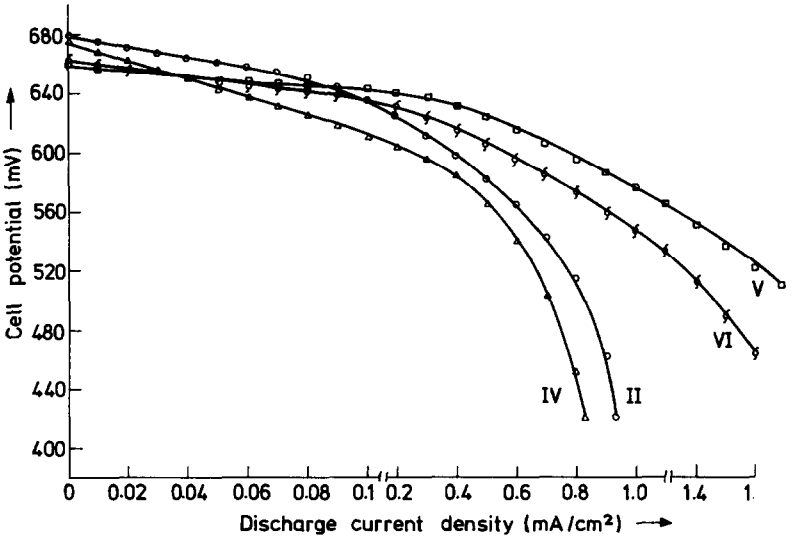

Fig. 8. Pulsed current discharge characteristic curves for the amorphous electrolyte cells II (○), IV (△), V (□), VI (§).

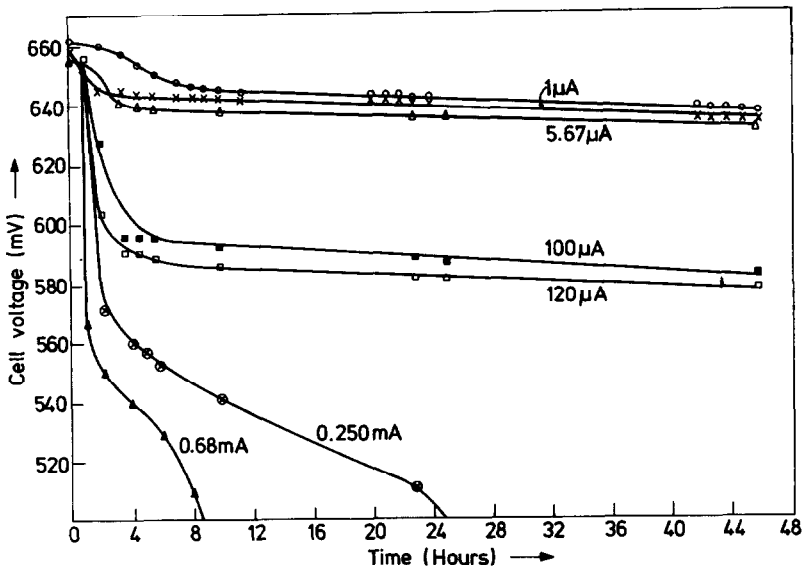

Fig. 9. Galvanostatic discharge profiles with time at various currents in cell V, where × = 1 μA, △ = 5.67 μA, ■ = 100 μA, □ = 120 μA, ○ = 0.250 mA, ▲ = 0.68 mA.

An improvement in the cathode–electrolyte interface is being considered by implementing various organic charge-transfer-complexing cathode materials and inorganic-insertion rechargeable cathodes that may undergo intercalation/de-intercalation of Ag^+ ion, and thus result in rechargeable cells. These studies seem to be more promising with the recent developments on photo-rechargeable batteries [14–16], where the possibility of obtaining low photovoltage (about 0.6 V) from a photo-electrochemical cell can be integrated into a rechargeable silver anode/insertion cathode, solid-state thin-film battery to de-intercalate the silver ions in the cathode, thus charging the battery with the generated photocurrent.

List of symbols

GF Glass former
GM Glass modifier
X AgI content
y Glass modifier content
z Glass former content
z/y GF/GM ratio
T_g Glass transition temperature
σ Conductivity
σ_o Pre-exponential factor
k Boltzmann constant
E_a Activation energy

I Total current
I_e Current due to electrons
I_h Current due to holes
R Universal gas constant
T Absolute temperature
A Area of the cell
L Thickness of the cell
F Faraday constant
σ_e Electronic conductivity
E Applied potential
σ_h Hole conductivity
Ag Silver
I_2 Iodine
C Carbon

References

1 T. Takahashi, *J. Electrochem. Soc., 119* (1972) 477.
2 T. Takahashi, *J. Electrochem. Soc., 120* (1973) 647.
3 G. Chiodelli, A. Magistris and A. Schiraldi, *Electrochim. Acta, 19* (1974) 655.
4 B. Scrosati, F. Papaleo and G. Pistoia, *J. Electrochem. Soc., 122* (1975) 339.
5 T. Minami, Y. Ikeda and M. Tanaka, *J. Non-Cryst. Solids, 51* (1982) 159.
6 G. Chiodelli, A. Magistris and J. L. Bjorkstam, *J. Non-Cryst. Solids, 51* (1982) 143.
7 T. Minami, *J. Non-Cryst. Solids, 56* (1983) 15.
8 K. Hariharan, C. V. Tomy and R. Kaushik, *J. Mater. Sci., Lett., 4* (1985) 1379.
9 B. V. R. Chowdari and R. Gopalakrishnan, *Solid State Ionics, 18/19* (1986) 483.
10 A. N. Durga Rani and K. Hariharan, *Solid State Ionics, 28/30* (1988) 799.
11 P. Sathya Sainath Prasad and B. Rambabu, *J. Mater. Sci., 26* (1991) in press.
12 P. Sathya Sainath Prasad and B. Rambabu, *J. Mater. Sci., Lett., 9* (1990) 1066.
13 D. Majumdar, P. A. G. Acharyulu and D. N. Bose, *J. Phys. Chem. Solids, 43* (1982) 933.
14 H. Tributsch, *Appl. Phys., 23* (1980) 61.
15 T. A. Skotheim and O. Inganas, *J. Electrochem. Soc., 132* (1985) 2116.
16 A. Turkvoc, *Solid State Ionics, 28* (1988) 900.